EPJ Web of Conferences **292**, 06002 (2024) https://doi.org/10.1051/epjconf/202429206002
NRM2023

Application of the semiclassical distorted wave model to the inclusive $(d, d'x)$ reaction

Hibiki Nakada[1,*], *Kazuki* Yoshida[2], and *Kazuyuki* Ogata[3,1]

[1]Research Center for Nuclear Physics, Osaka University, Ibaraki, Osaka 567-0047, Japan
[2]Advanced Science Research Center, Japan Atomic Energy Agency, Tokai, Ibaraki 319-1195, Japan
[3]Department of Physics, Kyushu University, Fukuoka 819-0395, Japan

Abstract. We apply the semiclassical distorted wave model to the deuteron-induced inclusive $(d, d'x)$ reaction. The calculated double differential cross sections (DDXs) as a function of the deuteron emission energy and the scattering angle are compared with experimental data. The calculated DDXs reasonably reproduce experimental data in the small energy-transfer region and at the forward angles. It is found that the refraction, which is the changes in the kinematics of the deuteron inside a nucleus, is necessary to reasonably reproduce the experimental data. We show that the refraction causes the increase/decrease in the differential cross section of the elementary process, hence the DDX.

1 Introduction

Multi-step direct (MSD) processes are important because they give a major contribution to the energy spectra of emitted particles at intermediate energies. The semiclassical distorted wave model (SCDW) [1–6], which has no free adjustable parameter, has been successful in describing MSD processes. SCDW has two notable features. First, SCDW adopts the local Fermi gas model (LFG) for the initial and final nuclear single-particle (s.p.) states. Although LFG is not practical for modeling specific nuclear states, it will reasonably describe the entire response of nuclei in the inclusive reactions. Second, the kinematics of the incoming and outgoing particles in the nucleus is properly treated by applying the local semiclassical approximation (LSCA) to the distorted waves of them. SCDW based on these two approximations permits an intuitive picture that the double differential cross section (DDX) of the inclusive reaction is an accumulation of the elementary processes that satisfy the energy and local-momentum conservation as well as the Pauli principle inside a nucleus. SCDW has been applied to $(p, p'x)$ and (p, nx) reactions incorporating up to the three-step processes [3], and the spin observables incorporating up to the two-step processes [4]. The latest version of SCDW adopts the Wigner transform of one-body density matrices calculated with a s.p. model for nuclei [5] instead of LFG.

On the other hand, few models describe MSD for deuteron-induced reaction because of the difficulty of describing deuteron breakup. Recently, the Kalbach model [7] and its extended model [8] have successfully reproduced experimental data in several cases. It should be noted, however, that the Kalbach model does not take into account the distortion of the incoming and outgoing particles and contains some free adjustable parameters.

*e-mail: nakada27@rcnp.osaka-u.ac.jp

© The Authors, published by EDP Sciences. This is an open access article distributed under the terms of the Creative Commons Attribution License 4.0 (https://creativecommons.org/licenses/by/4.0/).

The purpose of the present work is twofold. One is to test the validity of SCDW in the deuteron-induced inclusive reaction. As a first step, we apply the original SCDW including the one-step process [1], in which LFG and LSCA are used, to deuteron-induced inclusive $(d, d'x)$ reactions. Then, we compare the calculated DDXs with experimental data in the regions where the one-step process is dominant, i.e., the regions with the small energy transfer and at forward scattering angles, as discussed in SCDW studies for $(p, p'x)$ and (p, nx) [3]. The other is to investigate to what extent changes in the kinematics of the deuteron inside a nucleus affect the DDX. Such "refraction" effect is expected to be significant in the $(d, d'x)$ reactions because the distorting potential for the deuteron is strong compared to that for the nucleon.

2 Model

We describe the inclusive $(d, d'x)$ reaction with SCDW. The DDX for the energy E_f and the solid angle Ω_f of the emitted deuteron is expressed with [9]

$$\frac{\partial^2\sigma}{\partial E_f \partial\Omega_f} = \left[\frac{A_d A}{A_d + A}\right]^2 \frac{k_f}{k_i} \int d\boldsymbol{R}\, |\chi_f^{(-)}(\boldsymbol{R})|^2 |\chi_i^{(+)}(\boldsymbol{R})|^2 \left[\frac{\partial^2\sigma}{\partial E_f \partial\Omega_f}\right]_{\boldsymbol{R}} \rho(\boldsymbol{R}), \tag{1}$$

where A_d and A are the mass numbers of the deuteron and the target nucleus, respectively. k_i (k_f) is the asymptotic momentum of the incident (emitted) deuteron, $\boldsymbol{R}$ is the coordinate with respect to the center of the target nucleus. The distorted wave for the deuteron in the initial (final) state is denoted by χ_i (χ_f) and $\rho(\boldsymbol{R})$ is the nuclear density at $\boldsymbol{R}$. The averaged double differential cross section of the elementary process in the Fermi sphere at $\boldsymbol{R}$ is given by

$$\left[\frac{\partial^2\sigma}{\partial E_f \partial\Omega_f}\right]_{\boldsymbol{R}} = \frac{1}{(4\pi/3)k_F^3(\boldsymbol{R})} \left[\frac{A_d + 1}{A_d}\right]^2 \int_{k_\alpha \le k_F(\boldsymbol{R})} d\boldsymbol{k}_\alpha \left(\frac{d\sigma_{dN}}{d\Omega}\right)_{\theta_{dN}(\boldsymbol{R}), E_{dN}(\boldsymbol{R})} \delta(E_i + \varepsilon_\alpha - E_f - \varepsilon_\beta), \tag{2}$$

where $k_F(\boldsymbol{R})$ is the Fermi momentum at $\boldsymbol{R}$ and $\boldsymbol{k}_\alpha$ is the momentum of the nucleon in the target in the initial state. $d\sigma_{dN}/d\Omega$ is the free d-N differential cross section determined by the local scattering angle $\theta_{dN}(\boldsymbol{R})$ and the local scattering energy $E_{dN}(\boldsymbol{R})$ between the deuteron and the nucleon in the target. E_i is the deuteron incident energy, whereas ε_α (ε_β) is the kinetic energy of the nucleon in the target nucleus in the initial (final) state.

To investigate the refraction effect, instead of LSCA, we also consider the asymptotic momentum approximation (AMA), which approximates the momentum of the deuteron in the nucleus with the asymptotic one. Once AMA is applied, the elementary cross section in Eq. (2) is independent of $\boldsymbol{R}$, i.e., $\theta_{dN}(\boldsymbol{R}) \to \theta_{dN}$ and $E_{dN}(\boldsymbol{R}) \to E_{dN}$ as discussed in detail in Ref. [9].

3 Results

3.1 Comparison with experimental data

The deuteron-nucleus optical potential by An and Cai [10] is adopted for the deuteron-nucleus scattering in the initial and the final states. We assume the Woods-Saxon form for the nuclear density $\rho(\boldsymbol{R})$, and the radial parameter is given by $R_\rho = r_\rho A^{1/3}$ with $r_\rho = 1.15$ fm, and the diffuseness parameter is set to $a_\rho = 0.5$ fm as in Ref. [1]. As for the d-N differential cross

section, we use the numerical table of Ref. [11] obtained by fitting the experimental data of *p*-*d* elastic scattering with several Gaussian functions.

In Fig. 1, we show the emission-energy dependence of the DDXs of ^{27}Al$(d, d'x)$ for the laboratory scattering angles θ = (a) 10°, (b) 30°, (c) 60°, and (d) 90°; for systematic analysis, see Ref. [9]. The solid and dashed lines represent the calculated DDXs with LSCA and those with AMA, respectively. The experimental data are taken from Ref. [12]. In Fig. 1(c), the hump in the experimental data with $E_f \simeq 90$ MeV is due to the elastic scattering events.

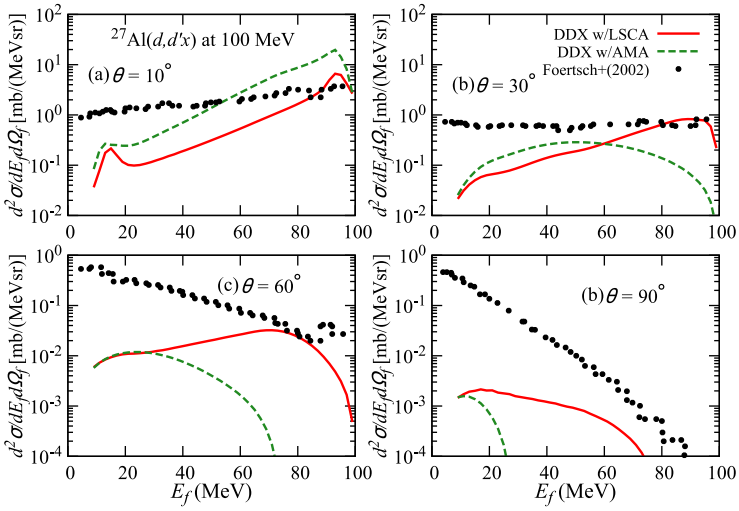

Figure 1. Comparison of the experimental data [12] and calculated DDXs of the inclusive ^{27}Al$(d, d'x)$ reaction at 100 MeV for different deuteron emission angles of (a) 10°, (b) 30°, (c) 60°, and (d) 90°. The solid (dashed) lines represent the DDXs with LSCA (AMA).

The contribution of multi-step processes, which is not included in the present calculation, becomes more pronounced as the energy transfer $\omega \equiv E_i - E_f$ or θ increases as discussed in Ref. [3] for the $(p, p'x)$ reaction. Therefore, we focus only on the regions with $\omega \leq 20$ MeV. In this region, the calculated DDXs with LSCA at θ = 10°, 30°, and 60° reasonably reproduce the experimental data. However, the DDX with LSCA at θ = 90° undershoots the data probably because of the missing of multi-step processes. On the other hand, those with AMA underestimate the experimental data even in the small ω region, except for the case of θ = 10°. By comparing the DDXs with LSCA and AMA, one can see that the inclusion of the nuclear refraction, i.e., the change in the kinematics of the deuteron inside the nucleus, is necessary to reproduce the experimental data reasonably.

Figure 2 shows the calculated DDX and the experimental data [13] of ^{58}Ni$(d, d'x)$ at 80 MeV as a function of the center-of-mass scattering angle $\theta_{c.m.}$ with ω = 10 MeV. The solid (dashed) line corresponds to the calculated DDX with LSCA (AMA). The angular distribution of the DDX with AMA is steep compared to that of the experimental data. On the other hand, the DDX with LSCA shows a better agreement with the data. From Fig. 2, it is evident that the refraction effect significantly changes the angular dependence of the DDX; it decreases the DDX at forward angles and increases at middle and backward angles.

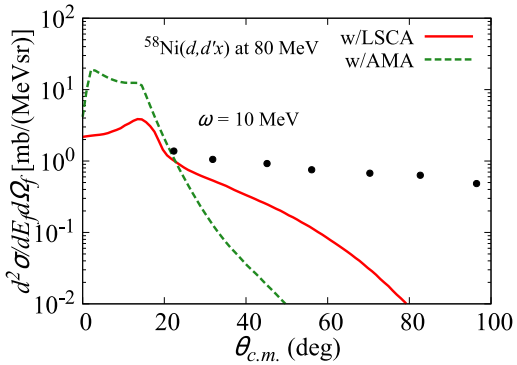

Figure 2. DDXs of ^{58}Ni($d, d'x$) at 80 MeV as a function of the center-of-mass scattering angle with ω = 10 MeV. The solid and dashed lines correspond to the calculations with LSCA and AMA, respectively. The experimental data are taken from Ref. [13].

3.2 Refraction effect on the elementary process

Below, we discuss the refraction effect on the DDX in the small ω region. The main reason for the change in the DDX due to the refraction effect is the difference in the kinetically allowed region of the elementary process, as discussed in Ref. [9]. Here, we discuss the secondary reason which is the momentum-transfer dependence (angular distribution) of the d-N cross section. Figure 3 shows the local momentum transfer $q(\boldsymbol{R})$ in the scattering plane of

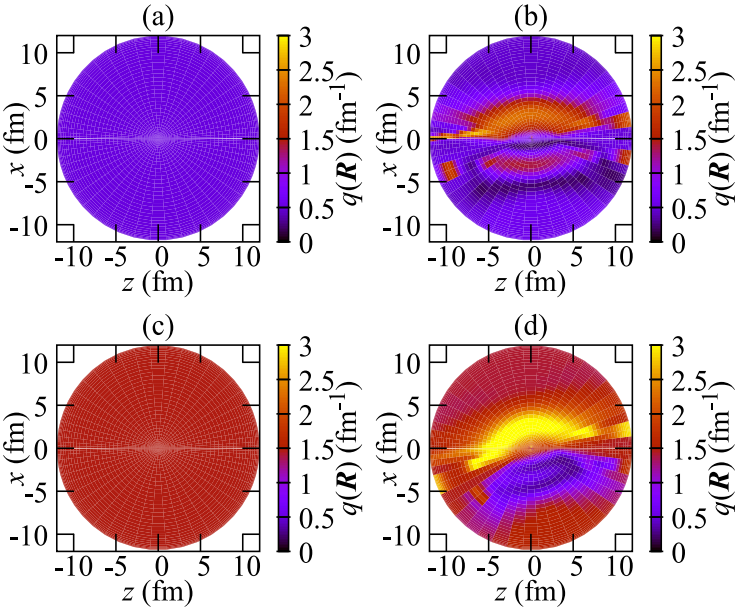

Figure 3. The local momentum transfer of ^{27}Al($d, d'x$) at 100 MeV with ω = 10 MeV at θ = 10° using (a) AMA and (b) LSCA, and at θ = 30° using (c) AMA and (d) LSCA.

^{27}Al($d, d'x$) at 100 MeV with ω = 10 MeV. The z axis is in parallel with the direction of the

incident deuteron. Figures 3 (a) and (b) show the local momentum transfers at $\theta = 10^\circ$ using AMA and LSCA, respectively, whereas (c) and (d) show them at $\theta = 30^\circ$. Trivially, $q(\boldsymbol{R})$ is independent of $\boldsymbol{R}$ in AMA. In LSCA, $q(\boldsymbol{R})$ is dispersed because of the refraction. Furthermore, $q(\boldsymbol{R})$ with LSCA at 10° has a broad region where $q(\boldsymbol{R})$ is larger than the asymptotic momentum transfer q. In contrast to the case with $\theta = 10^\circ$, $q(\boldsymbol{R})$ at $\theta = 30^\circ$ is smaller or larger than q, depending on $\boldsymbol{R}$.

The changes in $q(\boldsymbol{R})$ affect the d-N differential cross section contributing to the DDX as the elementary process. In Fig. 4, the solid, dashed, and dotted lines represent the d-N differential cross sections at deuteron incident energies $E_d = 80$, 100, and 120 MeV, respectively, as a function of the momentum transfer q. From this figure, it can be seen that the d-N differential cross sections tend to be larger when q is smaller. The d-N differential

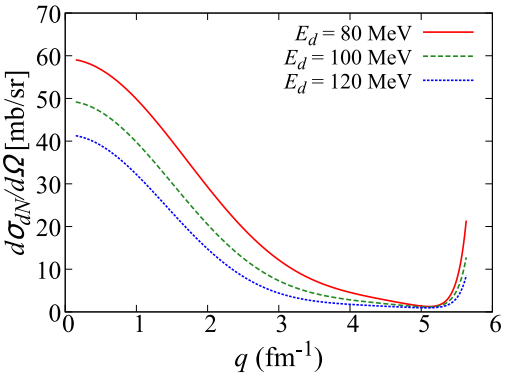

Figure 4. The elastic differential cross sections of d-N as a function of momentum transfer q. The solid, dashed, and dotted lines represent the cross sections with the deuteron incident energies E_d = 80 MeV, 100 MeV, and 120 MeV, respectively.

cross section of the elementary process contributing to the DDX of ^{27}Al$(d, d'x)$ at $\theta = 10^\circ$ with $\omega = 10$ MeV is about 48 mb/sr because $q(\boldsymbol{R})$ using AMA is about 0.5 fm^{-1} in the case as shown in Fig. 3(a). In LSCA, the smaller differential cross sections contribute to the DDX become smaller because, as discussed above, $q(\boldsymbol{R}) \geq q$ in almost all regions; see Fig. 3(b). On the other hand, at $\theta = 30^\circ$, differential cross sections contributing to the DDX become larger when LSCA is used because there is a region where $q(\boldsymbol{R}) < q$. This is a secondary mechanism by which the DDXs at forward (middle) angles are decreased (increased) by considering the refraction.

4 Summary

We have applied SCDW to the inclusive $(d, d'x)$ reaction. The calculated DDXs as a function of the deuteron emission energy are compared with the experimental data of ^{27}Al$(d, d'x)$ at several deuteron emission angles. The DDXs with LSCA show a reasonable agreement with the experimental data if the energy transfer ω and at the forward scattering angles θ are small, where the one-step process is expected to be dominant. On the other hand, the DDXs with AMA, which does not take into account the changes in the kinematics of the deuteron by the distorting potential, show too strong angular dependence and severely underestimate the experimental data for $\theta \geq 30^\circ$. The calculated DDXs of ^{58}Ni$(d, d'x)$ at 80 MeV as a function of the scattering angle with energy transfer $\omega = 10$ MeV are also compared with

the experimental data. This comparison clearly shows that the DDX with LSCA is in better agreement with the angular distribution of the experiment data than that DDX with AMA.

We have shown that the refraction effect changes the local momentum transfer of the *d*-*N* elementary process and hence the *d*-*N* cross section and the DDX. At $\theta = 10^\circ$, $q(\boldsymbol{R})$ tends to become larger when the refraction is taken into account, and it leads to a smaller cross section of the elementary process. On the other hand, at $\theta = 30^\circ$, $q(\boldsymbol{R})$ can become smaller, and it results in a larger cross section.

An extension of the present SCDW model will be a future work to include multi-step processes so as to reproduce the experimental data not only at forward θ and with small ω but also in wider range of θ and ω.

References

[1] Y.L. Luo, M. Kawai, Phys. Rev. C **43**, 2367 (1991)
[2] M. Kawai, H.A. Weidenmüller, Phys. Rev. C **45**, 1856 (1992)
[3] Y. Watanabe, R. Kuwata, S. Weili, M. Higashi, H. Shinohara, M. Kohno, K. Ogata, M. Kawai, Phys. Rev. C **59**, 2136 (1999)
[4] K. Ogata, M. Kawai, Y. Watanabe, S. Weili, M. Kohno, Phys. Rev. C **60**, 054605 (1999)
[5] S. Weili, Y. Watanabe, M. Kohno, K. Ogata, M. Kawai, Phys. Rev. C **60**, 064605 (1999)
[6] K. Ogata, Y. Watanabe, S. Weili, M. Kohno, M. Kawai, Nuclear Physics A **703**, 152 (2002)
[7] C. Kalbach, Phys. Rev. C **37**, 2350 (1988)
[8] C. Kalbach, Phys. Rev. C **71**, 034606 (2005)
[9] H. Nakada, K. Yoshida, K. Ogata, Phys. Rev. C **108**, 034603 (2023)
[10] H. An, C. Cai, Phys. Rev. C **73**, 054605 (2006)
[11] Y. Chazono, K. Yoshida, K. Ogata, Phys. Rev. C **106**, 064613 (2022)
[12] S. Förtsch, D. Ridikas, W. Mittig, H. Savajols, P. Roussel–Chomaz, G. Steyn, J. Lawrie, Journal of Nuclear Science and Technology **39**, 792 (2002)
[13] J.R. Wu, C.C. Chang, H.D. Holmgren, Phys. Rev. C **19**, 370 (1979)